IET Image Processing

Research Article

IET Journals
The Institution of Engineering and Technology

Accurate leukocoria predictor based on deep VGG-net CNN technique

ISSN 1751-9659
Received on 19th December 2018
Revised 26th August 2019
Accepted on 7th April 2020
E-First on 8th July 2020
doi: 10.1049/iet-ipr.2018.6656
www.ietdl.org

Boyina Subrahmanyeswara Rao[1] ✉

[1]*Department of Electronics and Communication Engineering, Swarnandhra College of Engineering and Technology, Kakinada, Narsapur, West Godavari District, AP, India*

✉ *E-mail: bsraosubrahmanyeswara@gmail.com*

Abstract: The most important part of digital image analysis is object classification. Nowadays, deep learning makes an enormous achievement in computer vision problems. So there has been a lot of interests in applying features learned by convolutional neural networks (CNNs) on general image recognition to more tasks such as object detection, segmentation and face recognition. Leukocoria detection is one of the serious challenges in infant retinal treatment. Leukocoria is represented as an abnormal white reflection appearing in the eyes of an infant suffering from retinoblastoma. This research proposes a deep Visual Geometry Group-net CNN classifier for automatic detection of leukocoria. The proposed classifier comprises pre-processing, feature extraction and classification. The deep CNN classifier contains convolution layer, pooling layer and fully connected layer with weights are developed on each image. Experimental results based on several eye images consist of ordinary and leukocoric from flicker, and it demonstrates that the proposed classifier provides better results with the accuracy of 98.5% and the error rate is below 2% which exceeds the current results.

1 Introduction

Retinoblastoma (RB) is a paediatric ocular cancer normally specified with leukocoria (white-eye pupillary reflex). A symptom of this leukocoria is the abnormal light reflection on the retina of the eye [1]. During this statics, the pupil of the eye is displayed as white rather than the normal black. In some other conditions, instead of this white reflection of the iris, it is turned into large at the darkroom [2]. Leukocoria is caused due to some other reasons like Retinopathy of Prematurity (ROP), Coat's disease, primary vitreous (PHPV) and Toxocara canis. These abnormalities should be treated at an early stage; otherwise, it leads to harmful diseases. At the last stage of leukocoria leads some harmful diseases known as retinopathy of prematurity, cataract, retinal vascular abnormality, retinal detachment, intraocular infection endophthalmitis, RB and retinal malformation [3, 4].

Detection and the diagnosis of the retina in image processing is an effectual task. This will be done with the recent techniques which are given in the below section: In digital image processing, segmentation is one of the detection methods in which it separates the normal and abnormal pixels with the help of diagnostic scanning methods [5]. For that, we have to consider CT (Computerised Tomography), MRI (Magnetic Resonance Imaging) and Bone scan. MRI scans provide a better result when compared to the CT scan. The reason for that is CT scan does not have edge details and these CT scan images have low intensity, and it cannot identify the small tumours presented at the scanned images. CT images are poor in quality while associating to another detection scheme that's why we cannot use this CT for the segmentation process [6, 7].

Fig. 1 *Normal and leukocoria eye images*

Image processing techniques also concentrate on some other detection schemes named Bone marrow aspiration, Lumbar puncture (spinal tap), X-rays, magnetic fields, sound waves, and biopsy [8]. During the biopsy treatment, a small sample from a tumour is analysed in the lab with the microscope identification. For the two conditions, this treatment is not considered in the real world, which is (1) it is harmful to the eye and (2) Threaten to spread in an outer layer of the eye. Occasionally, leukocoria is detected from the normal photographs which are taken from the ordinary cameras [9].

The variation of normal and abnormalities can be identified with the white and red reflexes. So the leukocoria can be recognised when compared it with the person having red and white reflexes since leukocoria is classified as an abnormal disease [10, 11]. The above-mentioned Fig. 1 shows normal and abnormal eye images. In some situation, the significances of the false-negative finding are taken into intensive for RB illustration. This leads to 3–4% newly born cancer and increases the infant mortality rate to 30,000 per year [12, 13].

Finally, these all medical treatments are taken into account for real-world application of machine learning. Machine learning and computational biology are used for autonomous and semi-autonomous functioning [14]. These are regularly aimed at the supervised and unsupervised estimation and prediction of frequent pathologies. Pathology consequences have incomplete use in the field of diagnosis and detection [15]. In such condition, machine learning is smeared to the sensitivity of syndrome based on data (similar towards noticeable recognition of leukocoria in digital images). These preceding reports require a variability of lenient processing methods: support vector machines (SVMs), neural networks (NNs), Bayesian statistical approaches to contribute to the recognition of a breast tumour in cervical cancers, mammograms, lung cancer and prostate cancer [16]. The specific significance is considered into the effective usage of NN for the discovery of melanoma, skin cancers [17]. All of these situations are smeared to measure the locations, wherever experienced specialists deliberately search for classifying the syndrome conditions. However, it has a certain progression in the image

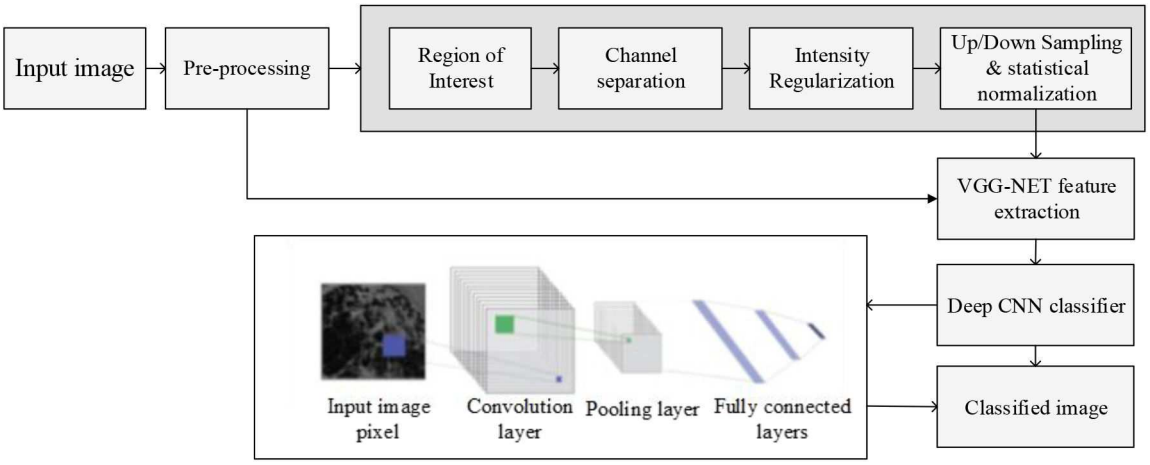

Fig. 2 *Proposed image classification for leukocoria detection*

processing, analysis of RB is extensively further challenging through opaque media or with abnormal structures [18–20].

In this paper, a deep VGG-net CNN (Visual Geometry Group-net Convolutional Neural Network) classifier is proposed which identifies a leukocoric eye using images processed to automatically recognise the faces, position of the eyes, Regions of Interest (ROI). Finally, an individual class for each eye uses deep convolutional neural network (CNN) classifiers to produce optimal outcomes. Here, we can show that this approach is a critical change over different techniques of machine learning-enabled leukocoria identification. This method accurately categorises the normal eye and the leukocoric eye from the dataset.

The remaining of the paper is described as follows. Section 2 describes the related works, and Section 3 explains the proposed approach of leukocoria detection. The performance analysis and conclusions are explained in Sections 4 and 5, respectively.

2 Related works

The most common symptom of Rb is a white reflection emitted from the retina and seen through the pupil. The reflection of light off the tumour causes the white colour. This symptom is called leukocoria and is present in 60% of reported Rb cases in the United States. Some of the recent work related to the automatic leukocoria detection in the machine learning-based image processing is given below.

Sun *et al.* [21] proposed a novel technique known as a red reflex test. This technique is suitable for evaluating the sensitivity of the red reflex. The red reflex test also validates RetCam fundus imaging, external inspection, and pupil examination and slit-lamp examination. The evaluation is performed for 7641 newborns, and it finds out the 18 undetected abnormalities in an eye.

Frenkel *et al.* [22] framed the scheme known as Multiplex Ligation-dependent Probe Amplification (MLPA). In which RB1 mutation presented at the retina was traced out. In addition to this MLPA, sequencing, and detection of recurrent CpG transition mutations are also performed. This performance is carried out by comparing normal tissues with the mutation presented tissues. This task reduces the risk of germline mutation analysis.

Dyer [23] introduces a novel idea of cell kind-particular syndrome vulnerability named 'cellular pliancy'. Furthermore removed the cancer tissue it evaded the cell with the degeneration process. During the treatment, it regenerates the cells with less harmful. This evaluation deliberates the significant pathway for RB search and it had designed the greatest present attempts in simple.

Mouw *et al.* [24] invented the frame work named Proton radiation therapy (PRT). Here leukocoria treatment is carried out for reducing the complexities of RB treatment. Here second malignancies and toxicity also reduced. In this process, childhood malignancies are not needed to treat the patient's outcomes. This technique was not suitable for long-term analysis.

Kartchner and Hartnett [25] presented the dual techniques named as Prompt laser therapy and lensectomy or vitrectomy. These two techniques are performed on the right and the left eyes for the medical analysis of FEVR. This technique avoids the complexities of wide-field fluorescein angiography with membrane dissection performance.

Rivas-Perea *et al.* [26] proposed a novel classification approach to detect leukocoria which is based on fuzzy logic with a number of classifiers. There are two transform approaches such as discrete cosine transform and Karhunen–Loeve transformation are used extract the features.

Henning *et al.* [27] proposed a CNN approach for classifying leukocoria, or white-eye reflections, in recreational photography. They also provide a method for tuning the outputs of a trained network to match desired true-positive (TPR)/false-positive rate (FPR).

The classifiers used in the literature were complex in large scale analysis, and the accuracy of detection is low. The error rate of classification in some models shows up to 11%. Early detection of recurrent leukocoria is critical for improved patient outcomes. So the enhancement of accurate detection is needed to achieve a better result.

3 Proposed methodology for deep VGG-net CNN classifier for leukocoria detection

Leukocoria detection is a severe challenge in the baby retinal treatment. The word leukocoria is perceived as 'amaurotic cat's eye'. This leukocoria also generated from the genomic function of the family members. Leukocoria should be treated at the early stage since it is very harmful and lead to retinoblastoma type cancer. Preliminary treatment and diagnosis of this Leukocoria is a challenging task. Testing plans like red reflex analysis takes more time for treatment and diagnosis. The initial finding of leukocoria through amateur photography might enable recent analysis [28]. As indicated by WHO, worldwide blindness due to leukocoria is around 1.5 million. Simply we have to introduce a measurable computer algorithm to treat the leukocoria at the early stage.

Going deep is the fundamental of deep learning and has exhibited an awesome achievement in many assignments. Both GooLeNet and VGGNet utilise very deep CNNs. Deep significantly enhances the learning capacity of the network. Although it has become a common sense to going deep, it is still unclear how to design a very deep CNN effectively. In this work, first, we propose a practical theory for designing very deep CNN effectively. The proposed scheme using deep CNN, which produces better classification results. For that, the image is to be pre-processed, and VGG-net extracts the features. The extracted features are classified with deep CNN, and it produces accurate results with low error. The purpose of this work is to achieve higher performance than other classifiers such as SVM, ANN (artificial NN). In this proposed work, eye images are taken for classification. Fig. 2 illustrates the VGG-net CNN classifier.

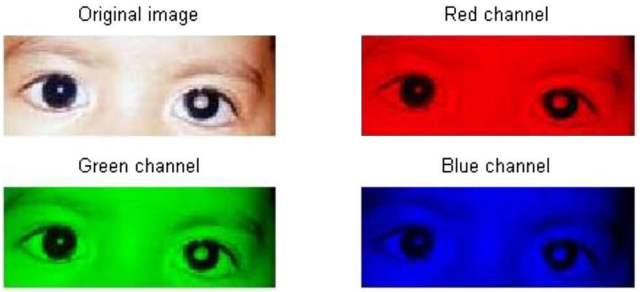

Fig. 3 *RGB plane separation*

3.1 Image pre-processing

Raw data if applied to any classification methods, do not produce good accuracy. So we need to pre-process the image before going to classification. In this work, the pre-processing consists of the below steps:

(i) *ROI:* An ROI is a piece of the image that is utilised for a particular reason. The input image is cropped, and the cropped image contains only $P \times Q$ RGB image of the periphery delimited by the iris. This procedure should be possible either automatically or manually.

(ii) *Channel separation:* RGB channel separation is the method that read the RGB channels separately. The image is denoted as $I(q_1, q_2, q_3)$, where $q_1 \in \{0, \ldots, P-1\}$, $q_2 \in \{0, \ldots, Q-1\}$ and $q_3 \in \{0, 1, 2\}$ are isolated into three grey-scale images $\{I_R(q_1, q_2), I_G(q_1, q_2), I_B(q_1, q_2)\}$, where (q_1, q_2) are the spatial dimension in a 2D image. $\{I_R(q_1, q_2), I_G(q_1, q_2), I_B(q_1, q_2)\}$ represent the red, green, blue colour values of the image at q_1, q_2 pixels, respectively. Splitting an image in its colour channels also decreases the time complexity of algorithms. Channel separation of the eye image is shown in Fig. 3.

(iii) *Intensity regularisation:* The DCT separates the images into parts. 2D-DCT model is applied to mitigate the variant illumination problem in the three channels. In an image $I(q_1, q_2)$ of size $P \times Q$, a matrix $\boldsymbol{G}_I(k_1, k_2)$ is determined and also the size consists of all spatial frequency components of the image, for $(k_1 \in (0, \ldots, P-1)$ and $k_2 \in (0, \ldots, Q-1))$. The matrix $\boldsymbol{G}_I$ processed with the 2D-DCT in the below manner:

$$\begin{aligned}\boldsymbol{G}_I(k_1, k_2) &= F(I(q_1, q_2)) \\ &= \alpha(k_1)\alpha(k_2) \sum_{q_1=0}^{P-1} \sum_{q_2=0}^{Q-1} I(q_1, q_2) \times \cos\left[\frac{\pi}{P}\left(q_1 + \frac{1}{2}\right)k_1\right] \\ &\quad \times \cos\left[\frac{\pi}{Q}\left(q_2 + \frac{1}{2}\right)k_2\right],\end{aligned} \tag{1}$$

where $F: \mathbb{R}^{P \times Q} \to \mathbb{R}^{P \times Q}$ and

$$\alpha(k) = \begin{cases} \sqrt{\frac{1}{Q}} & \text{for } k = 0, \\ \sqrt{\frac{2}{Q}} & \text{for } k \neq 0. \end{cases} \tag{2}$$

The first three coefficients of $F_I(k_1, k_2)$ will counter the variation of illumination inside the image, i.e. an updated frequency domain matrix $\widehat{\boldsymbol{F}}_I(k_1, k_2)$ is built by removing the elements in the coordinates $(k_1 = 0, k_2 = 0)$, $(k_1 = 1, k_2 = 0)$ and $(k_1 = 0, k_2 = 1)$ of F_I. After eliminating the first three DCT coefficients, $\widehat{\boldsymbol{F}}_I$ is inversely transformed from the frequency domain to the spatial domain as follows:

$$\begin{aligned}\widehat{\boldsymbol{I}}(q_1, q_2) &= F^{-1}\left\{\widehat{\boldsymbol{F}}_I(k_1, k_2)\right\} \\ &= \sum_{k_1=0}^{P-1} \sum_{k_2=0}^{Q-1} \alpha(k_1)\alpha(k_2)\widehat{\boldsymbol{F}}_I(k_1, k_2) \\ &\quad \times \cos\left[\frac{\pi}{P}\left(q_1 + \frac{1}{2}\right)k_1\right] \times \cos\left[\frac{\pi}{Q}\left(q_2 + \frac{1}{2}\right)k_2\right]\end{aligned} \tag{3}$$

where $F^{-1}: \mathbb{R}^{P \times Q} \to \mathbb{R}^{P \times Q}$ and $\alpha(\cdot)$ is also calculated with (2) and k is the kernel value.

(iv) *Up/down sampling:* Decreasing the file size, hence lower the pixel of the original image is called down-sampling the image. Increase the file size, hence enhancing the pixel of the original image is called up-sampling the image. Each image is then down-sampled or up-sampled to a fixed size of 64×64.

(v) *Statistical normalisation:* The technique which gives the normalised values or range of data from the original unstructured data using the concepts like mean and standard deviation then the parameter is called as Z-score normalisation. So the unstructured data can be normalised using Z-score parameter, as per the given formula:

$$F_i' = \frac{F_i - K}{\text{std}(K)} \tag{4}$$

where F_i' is the Z-score value, F_i is the row value of 'k' for the ith column. The below equation computes std(k).

$$\text{std}(k) = \sqrt{\frac{1}{(n-1)} \sum_{i=1}^{n} (F_i - \bar{k})^2} \tag{5}$$

here

$$\bar{k} = \frac{1}{n} \sum_{i=1}^{n} F_i \tag{6}$$

If suppose some row is having all the values are identical, so the standard deviation of that row is equal to zero then all values for that row are set to zero. After normalisation, the features are extracted by VGG-net.

3.2 VGG-net feature extraction

In this work, we explored the application of deep features extracted from VGG-Net for leukocoria detection task. VGG net is one of the most powerful deep CNNs. The runner-up in ILSVRC 2014 was the network from Karen Simonyan and Andrew Zisserman known as the VGG-Net. Its main contribution was showing the depth of the network is a critical component for good performance. Their final best network contains 16 CONV/FC layers that only performs 3×3 convolutions and 2×2 pooling from the beginning to the end.

3.3 Deep CNN classification

After feature extraction, a classifier is needed to find the corresponding label for each test image. There are various classifiers which can be used for this task such as SVM and NN. In this work, deep CNN has been used which is quite popular for image classification.

There are many modifications and adaptations to popular fully-connected feed-forward NNs. One adaptation is the CNN, which is well-suited for image-processing tasks. CNNs have been shown to significantly outperform many other state-of-the art algorithms for classification of images.

(i) *Convolutional layer:* Convolutional neuron layers are the key component of CNN. In image classification tasks, one or more 2D matrices (or channels) are treated as the input to the convolutional layer, and multiple 2D matrices are generated as the output. The number of input and output matrices may be different. The process to compute a single output matrix is defined as

$$\boldsymbol{O}_j = g\left(\sum_{i=1}^{n} \boldsymbol{M}_i \times \boldsymbol{km}_{i,j} + B_j\right) \tag{7}$$

Firstly each input matrix $\boldsymbol{M}_i$ is convoluted with a corresponding kernel matrix $\boldsymbol{km}_{i,j}$. Then the sum of all convoluted matrices is computed, and a bias value B_j is added to each element of the resulting matrix. Finally, a nonlinear activation function 'g' is applied to each element of the previous matrix to produce one output matrix $\boldsymbol{O}_j$.

Each set of kernel matrices represents a local feature extractor that extracts regional features from the input matrices. The aim of the learning procedure is to find sets of kernel matrices $\boldsymbol{K}$ that extracts good discriminative features to be used for image classification. The back propagation algorithm that optimises NN connection weights can be applied here to train the kernel matrices and biases as shared neuron connection weights.

1. *Pooling layer:* Pooling layer plays a major role in CNN for feature dimension reduction. To reduce the number of output neurons in the convolutional layer, pooling algorithms should be applied to combine the neighbouring elements in the convolution output matrices. Commonly used pooling algorithms include max-pooling and average-pooling. In this work, max-pooling layer with 2×2 kernel size selects the highest value from the four neighbouring elements of the input matrix to generate one element in the output matrix. During error back propagation process, the gradient signal must be only routed back to the neurons that contribute to the pooling output.
2. *ReLU neuron activation:* In our CNN model, the ReLU activation function is used in the convolutional layer. The ReLU activation function improves classification performance, and the network converges much faster than using the sigmoid activation function. In the NN, the basis function for input is obtained by the following equation:

$$B_i = \sum_{i=1}^{M} X_i W_{ij}^{I} \tag{8}$$

In the equation, X_i is the ith input value, W_{ij}^{I} is the weights assigned to the input and the hidden layers, and M is the total number of input neurons.

The activation function is obtained by the following equations:

$$H\_i = \frac{1}{1 + \exp(-B\_i)} \tag{9}$$

In the equation, H_i is the activation function and B_i is the basic function.

The output of the NN is obtained by the following equation:

$$Y = \sum_{j=1}^{N} \frac{W_{jd}^{O}}{1 + \exp\left(-\sum_{i=1}^{M} X_i W_{ij}^{I}\right)} \tag{10}$$

In equation, W_{jd}^{O} is the weight between hidden and the output layers, N is the total number of hidden neurons, and d is the number of outputs. From this (10) we can get the classification result.

A classification model for automatic leukocoria detection is designed. The illumination problems and colour variations are handled in the pre-processing stage. Deep features are extracted automatically using VGG-Net feature extraction. Then the proposed classifier that detects a leukocoric eye using images processed to detect leukocoria automatically. It provides better performance regarding classification accuracy.

4 Experimental results and analysis

In this section, provided the detailed description of our experimental results. The proposed technique has implemented in MATLAB. This research uses a database of digital images corresponding to the eyes of 62 faces, for a total of 124 eye images. This database is strictly an internal collection of images produced by the authors of this paper, consequently, no external permission is required. To the best of our knowledge, there are no other databases for this task. Out of the 124 eye images, 35 eyes are labelled as 'leukocoric' while the remaining 89 are labelled as 'healthy'.

Before presenting the results, let us describe the parameter values of our algorithm. For each image, we extract features from different layers of VGG-Net, from fc6 and some of the previous layers. The output of fc6 layer is a 4096-dimensional vector, but in the layers before that, we have 256/512 filter outputs of different sizes. We take the average of each filter output and form a feature vector from each layer to evaluate the performance of features extracted from different layers. Figs. 4–9 show the convolution features of normal and leukocoric eye images. Each figure contains seven parts which are DCT, z-score, convolution weight 1, weight 2, valid convolution, valid pooling and full convolution.

We have tested our work on leukocoria database which are retrieved from flickr library. We resize all images to 64×64 to be suitable for VGG-Net input. DCT and z-score are the pre-processed output of eye images. Then the convolution layers denote the number of trainable filters in each layer. Each first- and second-level convolutional layer is followed by a 2×2-pixel max-pooling layer to decrease the network dimension. Note that not every weight in a convolutional layer is independent replicated neurons have tied weights.

Performance metrics: The performance metrics of TPR, F-measure, G-mean measures, precision, confusion matrix, recall, kappa and ROC of the proposed method is compared with the existing classifiers. Such definitions allow us to use following performance metrics based on a confusion matrix:

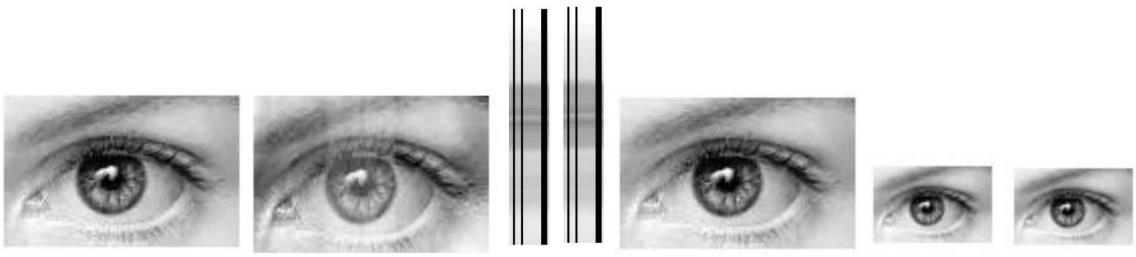

Fig. 4 *Normal eye of the red channel*

Fig. 5 *Leukocoric eye of the red channel*

$$\text{Accuracy} = \frac{\text{TP} + \text{TN}}{\text{TP} + \text{FN} + \text{FP} + \text{TN}} \tag{11a}$$

$$\text{TP rate or sensitivity or recall} = \frac{\text{TP}}{\text{TP} + \text{FN}} \tag{11b}$$

$$\text{TN rate or specificity} = \frac{\text{TN}}{\text{TN} + \text{FP}} \tag{11c}$$

$$\text{FP rate} = \frac{\text{FP}}{\text{TN} + \text{FP}} \tag{11d}$$

$$\text{Precision or positive predictive value} = \frac{\text{TP}}{\text{TP} + \text{FP}} \tag{11e}$$

$$\text{Negative predictive value} = \frac{\text{TN}}{\text{TN} + \text{FN}} \tag{11f}$$

$$\text{False discovery rate} = \frac{\text{FP}}{\text{FP} + \text{TP}} \tag{11g}$$

$$\text{Matthews correlation coefficient} = \frac{\text{TP} \times \text{TN} - \text{FP} \times \text{FN}}{\sqrt{(\text{TP} + \text{FP})(\text{TP} + \text{FN})(\text{TN} + \text{FP})(\text{TN} + \text{FN})}} \tag{11h}$$

$$F_1\text{-score} = 2 \times \frac{\left(\frac{\text{TP}}{\text{TP} + \text{FP}}\right) \times \left(\frac{\text{TP}}{\text{TP} + \text{FN}}\right)}{\left(\frac{\text{TP}}{\text{TP} + \text{FP}}\right) \times \left(\frac{\text{TP}}{\text{TP} + \text{FN}}\right)} \tag{11i}$$

$$\text{Balanced error rate} = \frac{1}{2}\left(\frac{\text{FP}}{\text{TN} + \text{FP}} + \frac{\text{FN}}{\text{FN} + \text{TP}}\right) \tag{11j}$$

Equations (11a)–(11k) describe the performance measures for classification, where TP is truly positive, TN is a true negative, FP is false positive, and FN is a false negative. Table 1 shows the performance metrics of proposed classifier with traditional classifiers such as SVM and ANN. This helps to rank the classifiers. The table shows that the FPR, false discovery rate and the balanced error rate provide low value in contrast with other classifiers.

In this application, it is important to control FP predictions so that a user takes predictions of leukocoria seriously. To that end, we develop a method of tuning the outputs of a trained network to manipulate its receiver operator characteristics (ROC). On a ROC curve

$$X\text{-axis represents \%FP} = \frac{\text{TN}}{\text{TN} + \text{FP}} \tag{12a}$$

$$Y\text{-axis represents \%TP} = \frac{\text{TP}}{\text{TP} + \text{FN}} \tag{12b}$$

5 Results

The results of deep VGG-net CNN classifier are shown below. The horizontal axis describes the various approaches and the vertical axis describes the performance of the test set. The blue bar represents the proposed classifier; green bar shows the SVM classifier and red bar illustrates the ANN classifier.

Fig. 10 illustrates the analysis of classification accuracy and sensitivity for three techniques. The proposed deep CNN classifier achieve 98% accuracy on the data set. By using SVM techniques, the accuracy is 84%, and the ANN has 84% accuracy. The extraction of deep features provides better accuracy for the proposed work. The analysis of specificity, i.e. true negative rate also shown in the above figure. It measures the proportion of negatives that are correctly identified. Our deep CNN achieves

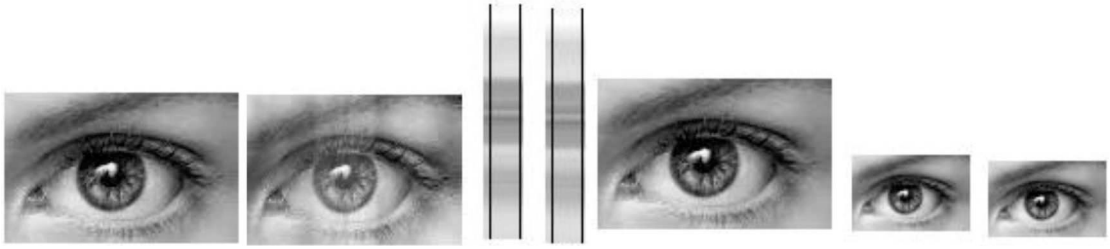

Fig. 6 *Normal eye of the green channel*

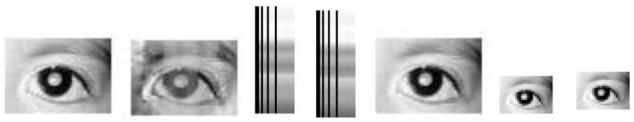

Fig. 7 *Leukocoric eye of the green channel*

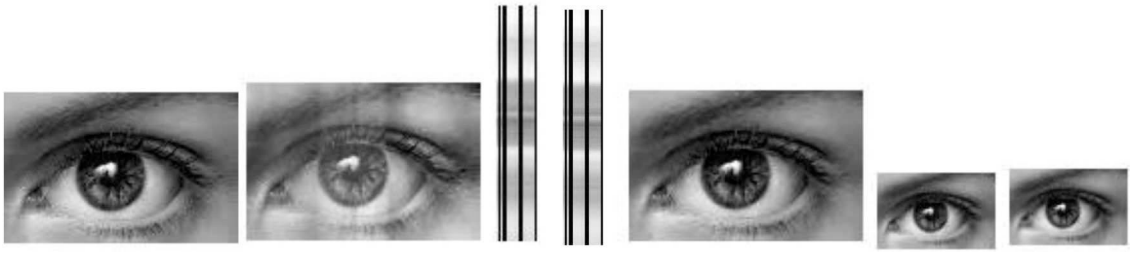

Fig. 8 *Normal eye of the blue channel*

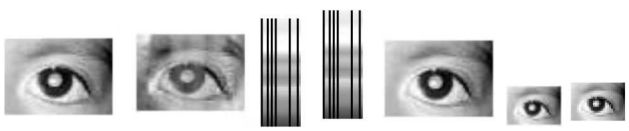

Fig. 9 *Leukocoric eye of the blue channel*

Table 1 Performance analysis of classifiers

Metrics	Deep CNN	SVM	ANN
accuracy	0.9856	0.842	0.845
sensitivity	0.9756	0.831	0.883
specificity	0.6377	0.860	0.773
FPR	0.1454	0.123	0.127
positive predictive value	0.9831	0.908	0.867
negative predictive value	0.4983	0.753	0.806
false discovery rate	0.0163	0.096	0.133
Matthews correlation coefficient	0.5572	0.476	0.467
F_1-score	0.8951	0.897	0.877
balanced error rate	0.0322	0.123	0.175

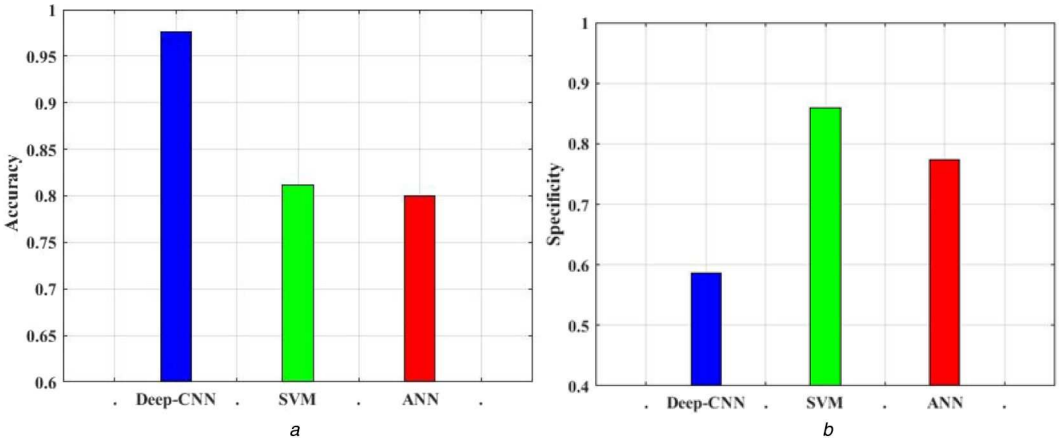

Fig. 10 *Accuracy and specificity analysis*
(a) Accuracy analysis, ***(b)*** Specificity analysis

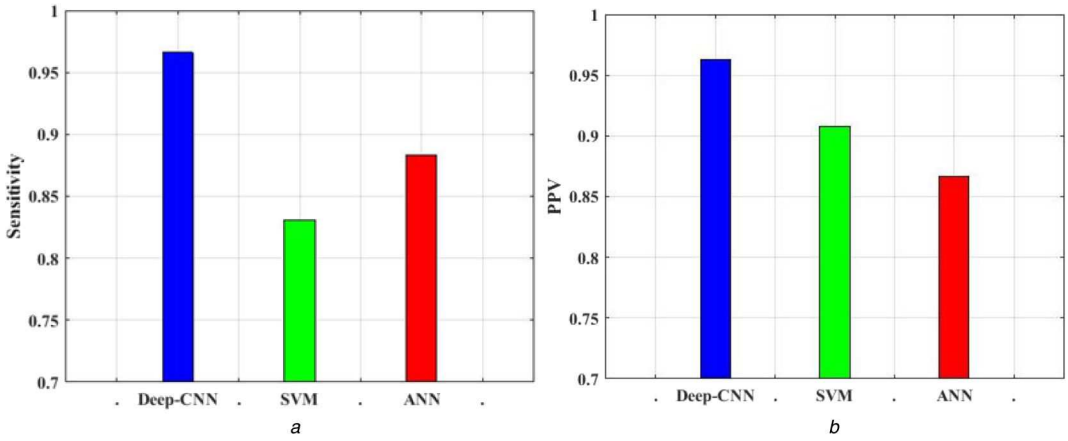

Fig. 11 *Sensitivity and positive predictive value analysis*
(a) Sensitivity analysis, ***(b)*** Positive predictive analysis

good performance than the existing classifiers. The specificity of deep CNN decreases when the sensitivity increases.

Fig. 11 describes the sensitivity analysis. The sensitivity of a test (also called the true positive rate) is defined as the proportion of people with the leukocoria who will have a positive result. In this proposed work performed well and achieved 97% and the existing classifiers provide 83, 88%, respectively. In addition, the figure depicts the performance of positive predictive analysis. It is the probability that the leukocoria is present when the test is positive. The deep CNN achieves high value in contrast with the other classifiers. The deep features from VGG-net provide accurate classification in the proposed classifier. Positive predictive value achieves 98% in the proposed and the SVM, ANN provides 90, 86% appropriately.

Fig. 12 demonstrates the negative predictive value. It compares the proposed work with traditional SVM and ANN classifiers. The proposed classifier provides low value than the existing. It is the greater achievement of classification. The execution analysis of various classifiers is also shown in this figure. The proposed deep CNN take little more time than other two classifiers because of the number of layers.

Fig. 13 illustrates the memory usage of various nets. The memory size of VGG-16 is high but its usage is low. So it gives better performance than the other nets. The yellow triangle represents the maximum layer wise usage.

6 Discussion

Table 1 provides a comparison of the performance of the proposed scheme and those of other recent algorithms on flicker. By using the deep features, we were able to achieve the highest accuracy rate on this data set. This is mainly due to the richness of deep features which can capture many of the information lost in hand-crafted features, providing a very high discriminating power.

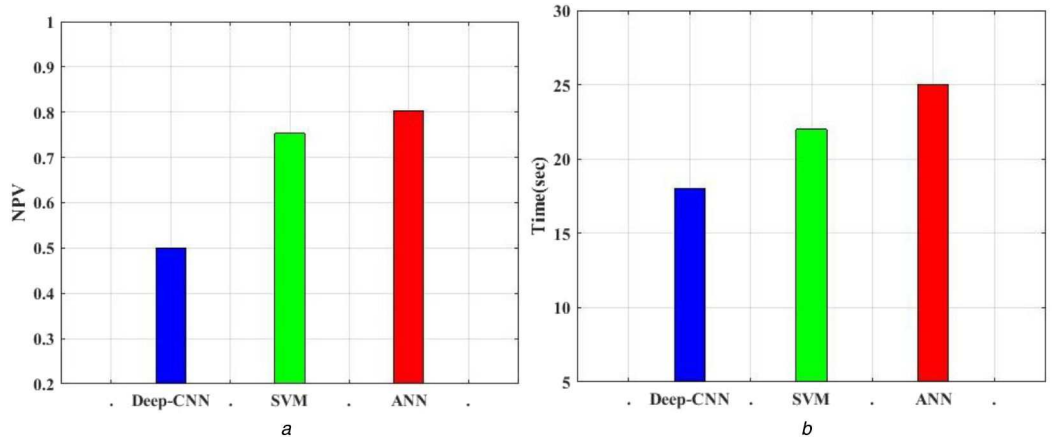

Fig. 12 *Negative predictive value and execution time analysis*
(a) Negative predictive analysis, ***(b)*** Execution time analysis

Several experiments were carried out to evaluate the suitability of proposed method for leukocoria detection. We compared our classification results with two other approaches. SVM and ANN classifiers also considered and implemented for prediction. SVMs are the lack of transparency of results. Using ANN for classification model learning has the distinct advantage that back-propagation algorithm can be applied to fine tune parameters in all layers to obtain a better final classification model. As shown in Figs. 10–13, our deep CNN classifier achieved the better classification performance.

Deep CNN is more efficient than deep NNs. This paper uses various pre-processing method for enhancing the performance of classification. Experimental results in Table 1 demonstrate the comparison of proposed classifier and the state-of-the-art models in leukocoria classification is illustrated in Table 2.

From the table, our proposed model accomplishes good precision and recall. We achieved low error rates (<2%) for classification of eye images into two classes such as normal and leukocoric. We show that it is possible to identify leukocoria in raw digital images of cropped eyes by training CNNs. Our solution can accurately recognise between two classes of eye image. Deep CNNs have been appeared to beat numerous other existing algorithms for classification of images essentially. One can identify the performance metric based on the area under ROC curve. It provides a basis judging whether a classifier performs well or not regarding TPR and FPR.

Figs. 10–13 demonstrate that the proposed classification scheme performs better than the other two techniques much of the time. The outcomes show that classifiers that use the VGG-net better than traditional classifier also, the TPR and FPR exhibit the better execution. A deep VGG-net CNN classifier is a good option in the detection of leukocoria in the eyes of infants with good accuracy.

7 Conclusion

In this work, a novel deep CNN-based method is proposed for image classification and compared with ANN and SVM based classifiers. Deep CNN is an excellent tool for detecting leukocoria. It produces better result than the traditional methods due to the deep features. We evaluated the application of deep features, extracted from VGG-net, followed by a simple classification algorithm for the problem of leukocoria detection. After that, classification is done using deep CNN classifier to generate a knowledge base. After extracting the features, training and testing samples are classified using deep CNN classifier to obtain the statistical data for proper image analysis. Our proposed method provides better performance by comparing with the conventional techniques.

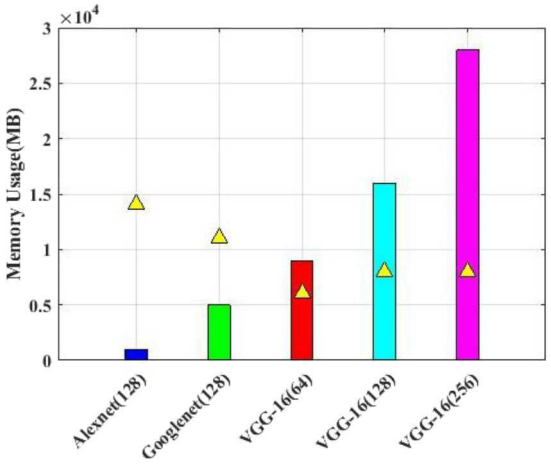

Fig. 13 *Memory usage analysis*

Table 2 Comparison with state-of-the-art methods

Metrics	Fuzzy-based soft fusion [26], %	CNN [27], %	Proposed approach, %
accuracy	92	94	98
TPR	89	91	95
FPR	11	7	2

8 References

[1] Patel, H.R., Bhaleeya, S.: 'Approach to leukocoria', in Medina Mendex, C.A., Townsend, J.H., Singh, A.D. (eds): '*Manual of retinal diseases*' (Springer International Publishing, Cham, Switzerland, 2016), pp. 47–50

[2] Chantada, G.L., Leal-Leal, C., Stefan, D.C., *et al.*: 'Retinoblastoma: international perspective', in '*Clinical ophthalmic oncology*' (Springer Berlin Heidelberg, Cham, Germany, 2015), pp. 51–60

[3] Yousef, Y.A., Shroff, M., Halliday, W., *et al.*: 'Detection of optic nerve disease in retinoblastoma by use of spectral domain optical coherence tomography', *J. Am. Assoc. Pediatric Ophthalmol. Strabismus*, 2012, **16**, (5), pp. 481–483

[4] Rivas-Perea, P., Henning, R., Shaw, B., *et al.*: 'Finding the smallest circle containing the iris in the denoised wavelet domain'. Image Analysis and Interpretation (SSIAI), San Diego, CA, USA, 6 April 2014, pp. 13–16

[5] Arai, E., Fujimaki, T., Yanagawa, A., *et al.*: 'Familial cases of norrie disease detected by copy number analysis', *Jpn. J. Ophthalmol.*, 2014, **58**, (5), pp. 448–454

[6] Ahani, A., Behnam, B., Khorshid, H.R., *et al.*: 'RB1 gene mutations in Iranian patients with retinoblastoma: report of four novel mutations', *Cancer Genet.*, 2011, **204**, (6), pp. 316–322

[7] Neudorfer, M., Waisbourd, M., Buzi, S., *et al.*: 'Color Doppler imaging of eyes with persistent fetal vasculature', *Pediatr. Radiol.*, 2012, **42**, (10), pp. 1229–1234

[8] Mahajan, A., Crum, A., Johnson, M.H., *et al.*: 'Ocular neoplastic disease', *Semin. Ultrasound, CT MRI*, 2011, **32**, (1), pp. 28–37

[9] Gombos, D.S.: 'Retinoblastoma in the perinatal and neonatal child', *Semin. Fetal Neonatal Med.*, 2012, **17**, (4), pp. 239–242

[10] Chévez-Barrios, P., Gombos, D.S.: 'Clinical features, diagnosis, pathology', in '*Retinoblastoma*' (Springer US, Boston, USA, 2010), pp. 25–40

[11] Pichi, F., Lembo, A., De Luca, M., *et al.*: 'Bilateral retinoblastoma: clinical presentation, management and treatment', *Int. Ophthalmol.*, 2013, **33**, (5), pp. 589–593
[12] Parulekar, M.V.: 'Retinoblastoma current treatment and future direction', *Early Hum. Dev.*, 2010, **86**, (10), pp. 619–625
[13] Zhang, L., Jia, R., Zhao, J., *et al.*: 'Novel mutations in the RB1 gene from Chinese families with a history of retinoblastoma', *Tumor Biol.*, 2015, **36**, (4), pp. 2409–2420
[14] Ansari, M.W., Nadeem, A.: 'Congenital anomalies of eye', in '*Atlas of ocular anatomy*' (Springer International Publishing, Cham, Switzerland, 2016), pp. 99–101
[15] De Francesco, S., Galluzzi, P., Bracco, S., *et al.*: 'Alternated intra-arterial and intravitreal chemotherapy for advanced intraocular retinoblastoma: preliminary successful results without systemic chemotherapy', *Int. Ophthalmol.*, 2015, **35**, (6), pp. 887–895
[16] Epelman, S.: 'Preserving vision in retinoblastoma through early detection and intervention', *Curr. Oncol. Rep.*, 2012, **14**, (2), pp. 213–219
[17] Samara, W.A., Pointdujour-Lim, R., Say, E.A., *et al.*: 'Foveal microanatomy documented by SD-OCT following treatment of advanced retinoblastoma', *J. Am. Assoc. Pediatric Ophthalmol. Strabismus*, 2015, **19**, (4), pp. 368–372
[18] Gombos, D.S.: 'Retinoblastoma in the perinatal and neonatal child', *Semin. Fetal Neonatal Med.*, 2012, **17**, (4), pp. 239–242
[19] Dimaras, H., Rushlow, D., Halliday, W., *et al.*: 'Using RB1 mutations to assess minimal residual disease in metastatic retinoblastoma', *Transl. Res.*, 2010, **156**, (2), pp. 91–97
[20] Kim, R.M., Park, S.E., Oh, S.: 'Clinical feature analysis of congenital optic nerve abnormalities', *Jpn. J. Ophthalmol.*, 2006, **50**, (3), pp. 250–255
[21] Sun, M., Ma, A., Li, F., *et al.*: 'Sensitivity and specificity of red reflex test in newborn eye screening', *J. Pediatr.*, 2016, **179**, pp. 192–196
[22] Frenkel, S., Zloto, O., Sagi, M., *et al.*: 'Genotype-phenotype correlation in the presentation of retinoblastoma among 149 patients', *Exp. Eye Res.*, 2016, **146**, pp. 313–317
[23] Dyer, M.A.: 'Lessons from retinoblastoma: implications for cancer, development, evolution, and regenerative medicine', *Trends Mol. Med.*, 2016, **22**, (10), pp. 863–876
[24] Mouw, K.W., Yeap, B.Y., Caruso, P., *et al.*: 'Analysis of patient outcomes following proton radiation therapy for retinoblastoma', *Adv. Radiat. Oncol.*, 2017, **2**, (1), pp. 44–52
[25] Kartchner, J.Z., Hartnett, M.E.: 'Familial exudative vitreoretinopathy presentation as persistent fetal vasculature', *Am. J. Ophthalmol. Case Reports*, 2017, **6**, pp. 15–17
[26] Rivas-Perea, P., Baker, E., Hamerly, G., *et al.*: 'Detection of leukocoria using a soft fusion of expert classifiers under non-clinical settings', *BMC Ophthalmol.*, 2014, **14**, (1), p. 110
[27] Henning, R., Rivas-Perea, P., Shaw, B., *et al.*: 'A convolutional neural network approach for classifying leukocoria'. 2014 Southwest Symp. on Image Analysis and Interpretation, San Diego, CA, USA, 2014, pp. 9–12
[28] Apushkin, M.A., Apushkin, M.A., Shapiro, M.J., *et al.*: 'Retinoblastoma and simulating lesions: role of imaging', *Neuroimaging Clin. N Am.*, 2005, **15**, (1), pp. 49–67